



Electrically controllable g tensors in quantum dot molecules

Till Andlauer and Peter Vogl

Walter Schottky Institut, Technische Universität München, 85748 Garching, Germany

(Received 2 October 2008; revised manuscript received 13 December 2008; published 15 January 2009)

We present a quantitative theoretical analysis of electron, hole, and exciton g tensors of vertically coupled InAs/GaAs quantum dot pairs in external electric and magnetic fields. For magnetic fields lying in the growth plane, we predict a giant electrically tunable anisotropy of hole g factors that is introduced by piezoelectric charges. This effect allows bias controlled g factor switching and single-spin manipulations in a static magnetic field. We use a relativistic eight-band $\mathbf{k}\cdot\mathbf{p}$ envelope function method including strain, which accounts for magnetic fields in a gauge-invariant manner. In a regime where the molecular wave functions form bonding and antibonding orbitals and for vertical magnetic fields, our results reproduce experimentally observed resonant enhancements of exciton g factors without any fitting parameters.

DOI: [10.1103/PhysRevB.79.045307](https://doi.org/10.1103/PhysRevB.79.045307)

PACS number(s): 73.21.La, 71.70.Ej, 75.75.+a, 03.67.Lx

I. INTRODUCTION

Spins of confined carriers in quantum dots are promising candidates for the logical units in quantum computers.¹⁻³ In many concepts developed so far, the individual spin qubits are being manipulated by magnetic fields,⁴ which is difficult to achieve in practice. An alternative procedure is to address individual spin qubits by their own electric gate⁵ which allows fast changes of the spin splitting, quantum gate operations, and a tuning of the spin storage time.³ In any case, progress in this field requires a detailed understanding of the mechanisms that allow one to modify the spin-related electronic structure properties such as gyromagnetic factors. In heterostructures, the possibility of electric control of g factors has been demonstrated by shifting the wave functions between different material regions by an applied bias.^{6,7} Together with the anisotropy of the g tensor, such an electrically controlled tuning of the Zeeman splittings allows spin manipulations without time-dependent magnetic fields.⁸ These experiments have been important proofs of principle but still represent ensemble averages. In quantum dots, electron and hole g factors have been extensively studied experimentally^{9,10} and theoretically.¹¹⁻¹³ In self-assembled dots, the g factors have been found to be almost isotropic within the growth plane.^{14,15} In addition, the tunability of quantum dot g factors, which has been investigated both theoretically¹⁶ and experimentally,¹⁷ is rather limited because the bound quantum dot wave functions are fairly insensitive to applied electric fields. By contrast, distinctive electrically tuned resonances have been discovered in recent experiments for the exciton g factors in vertically stacked quantum dot molecules.¹⁸ It is plausible that coupled quantum dots provide more room for shifting the electron and hole wave functions between the two quantum dots by an external electric field. Indeed, the authors have been able to explain their results in terms of a simple phenomenological model based on the bonding and antibonding nature of the molecular states.¹⁸

In this paper, we significantly extend the theoretical analysis of quantum dot molecules by showing that the piezoelectric polarization associated with stacked quantum dots produces a giant electrically tunable *in plane* anisotropy

of hole g factors. This g factor modulation is an order of magnitude larger than in individual quantum dots and effectively allows g factor switching between almost zero and a constant finite value by a single electric gate. We provide a general and quantitative theoretical analysis of the electric field dependent electron, hole, and exciton g tensors of coupled quantum dots. For vertical magnetic fields, we show that our calculated results reproduce the experimentally observed exciton g factors in Ref. 18 without any fitting parameters.

The paper is organized as follows. In Sec. II, we discuss the method employed for our calculations of the electron, hole, and exciton g tensors in quantum dot molecules. Results for the bias driven tuning of g factors in vertical magnetic fields are given in Sec. III. Here, we also compare our results with experimental data.¹⁸ In Sec. IV, we show that g tensor components can be switched on and off by an electric field and study the tunability of the g tensor anisotropy in lateral magnetic fields. These results are used to propose a universal single-spin qubit gate in Sec. V. In Sec. VI, resonant electron g factors in molecules with larger dot separation are studied. Finally, the results are summarized in Sec. VII.

II. METHOD

The realistic calculation of band-edge g factors of a self-assembled quantum dot molecule requires a solution of the Schrödinger equation for a mesoscopic system. It must include the substrate, the wetting layers, as well as the overgrown quantum dots, and must take into account the macroscopic strain field, the piezoelectric polarization, as well as any applied magnetic and electric fields. Only recently it has been recognized that an accurate incorporation of the magnetic field into the Schrödinger equation requires special care to ensure gauge-invariant results.¹¹⁻¹³ Since a key point of this paper lies in the tuning of g factors by an applied bias, both a magnetic and an electric field will be incorporated into the Schrödinger equation. We calculate the energies of electron and hole ground and first-excited states of the entire mesoscopic system using a relativistic eight-band $\mathbf{k}\cdot\mathbf{p}$ enve-

lope function method that has been described in detail in Ref. 13 and has been implemented into the simulation package nextnano.^{19,20} The Hamiltonian can be written schematically in the form

$$\hat{H} = \hat{H}_{\mathbf{k},\mathbf{p}}^{8 \times 8}(\mathbf{x}, \mathbf{x}', \mathbf{B}) + \frac{g_0 \mu_B}{2} \hat{\mathbf{S}}^{8 \times 8} \cdot \mathbf{B} + e\mathbf{x} \cdot \mathbf{F}, \quad (1)$$

where the first term on the right-hand side represents the eight-band effective-mass Hamiltonian of the entire structure in a discrete real-space basis (embracing N grid nodes). This term includes the coupling to the magnetic field \mathbf{B} in a manifestly gauge-invariant manner with \mathbf{B} only appearing in phase factors.¹³ Strain effects are incorporated into the Hamiltonian via linear band-edge deformation potentials¹³ and piezoelectric charges. The three-dimensional strain field is calculated by globally minimizing the total elastic energy,

$$E_\varepsilon = \int_V dV \frac{1}{2} C_{ijkl} \varepsilon_{ij} \varepsilon_{kl} \quad (i, j, k, l \in \{x, y, z\}), \quad (2)$$

employing a continuum elasticity model.²¹ Here, ε_{ij} and C_{ijkl} denote the elements of the strain and elasticity tensor, respectively. The material dependent coefficients are taken from Ref. 22. We assume the material interfaces to be characterized by pseudomorphic growth. In addition, we assume vanishing normal stress at the boundaries of the simulation domain. For localized nanostructures embedded into a substrate, the size of this three-dimensional domain is increased until the lattice has relaxed to the unstrained substrate on all boundaries. For the dots considered in this paper, this requires a domain size of the order of 100 nm along each axis. The piezoelectric charge density ρ_p is determined by the linear relation,²³

$$\rho_p = -\text{div } \mathbf{P} = -\partial_i e_{ijk} \varepsilon_{jk}, \quad (3)$$

with the piezoelectric tensor e_{ijk} . The material parameters are taken from Ref. 23. We have not included higher order piezoelectric effects since it was shown in Ref. 24 that such effects are negligible for quantum dots with smooth, realistic alloy profiles as considered in this paper. The second term on the right-hand side of Eq. (1) couples the spin to the field \mathbf{B} . Here, μ_B is the Bohr magneton, $g_0=2$ is the free-electron g factor, and the 8×8 spin matrices \hat{S}_i ($i \in \{x, y, z\}$) are completely determined by the Pauli matrices.¹³ The homogeneous electric field \mathbf{F} is assumed to point along the vertical [001] growth direction. All material parameters have been taken from Ref. 22 except for the Luttinger parameter κ that has been tabulated in Ref. 25. The $8N$ dimensional Hamiltonian does not include free-carrier charges but is augmented by the Poisson equation; in this way, the piezoelectric polarization is fully taken into account. We will focus on bound eigenstates of this Hamiltonian that are twofold Kramers degenerate at $\mathbf{B}=0$ and do not get split by inversion asymmetry effects. This applies to all s -type envelope states such as quantum dot ground states but not to some higher lying excited states, as has been discussed in detail in Refs. 26 and 27. For nonzero but small magnetic field, the states are subject to a Zeeman splitting that we find to depend linearly on the \mathbf{B} field up to approximately 10 T for the present struc-

tures. For energies close to the electron and hole band edges, respectively, the magnetic-field-dependent part of the Hamiltonian can be written as

$$\hat{H}_n = \frac{\mu_B}{2} \boldsymbol{\sigma} \cdot \hat{g}_n \cdot \mathbf{B}, \quad (4)$$

where \hat{g}_n ($n=e, h$) define the g tensors for the confined electron and hole states. The eigenvalues of this tensor yield the g factors $g_n = (E_n^\uparrow - E_n^\downarrow) / (\mu_B B)$. For both the electron and hole band edges, we focus on the ground (0) and first-excited (1) state. We note that the three-dimensional confinement of the molecular dot states causes these electronic states to be well separated from higher lying states so that this definition of g factors is unambiguous.

The g factor g_x of a neutral magnetoexciton X^0 is defined by the energy difference between the configurations $\sigma^+(e^\downarrow h^\uparrow)$ and $\sigma^-(e^\uparrow h^\downarrow)$, where electron and hole states have opposite spins,

$$g_x = \frac{E(\sigma^-) - E(\sigma^+)}{\mu_B B}. \quad (5)$$

We note that the other combinations of electron and hole states do not lead to optically active configurations. Since the electron-hole exchange energy is small compared to typical Zeeman splitting energies, we define the exciton g factors g_x^0 and g_x^1 for the lowest and first-excited magnetoexciton state by²⁸

$$g_x^0 = g_e^0 + g_h^0, \quad (6)$$

$$g_x^1 = g_e^0 + g_h^1, \quad (7)$$

where g_e^0 and g_h^0 are the electron and hole ground-state g factor, respectively. Since the hole states lie much denser than the electron states, the excitonic g factor g_x^1 involves the ground electron g_e^0 and first-excited hole g_h^1 .

For the concrete predictions presented in this paper, we consider vertically stacked InAs/GaAs double dot structures that have been fabricated and studied experimentally recently.^{29,30} The quantum dot molecule itself is characterized by the dot separation d , the quantum dot height h , the dot width w , and the alloy profile within the individual dots that we assume to have identical size and composition (see Fig. 1). We take $h=2.5$ nm, $w=15$ nm, $d=1.5$ or 2 nm, and a realistic^{32,33} trumped-shaped alloy profile throughout. This alloy profile is described in detail in Ref. 31 and is characterized by an indium distribution that starts from 100% at the tip, and decreases to 80% and 40% toward the bottom center and the bottom corners of the individual dots, respectively. We model the dots as truncated pyramids with {011} side facets that sit on 0.5 nm InAs wetting layers on a (001)-GaAs substrate. With these parameters, we find the lowest interband transition energy of the entire structure to be 1.30 eV for $d=1.5$ nm as well as $d=2$ nm. For this structure, we predict the principal axes of all g tensors to be given by the set [001], [110], and [1 $\bar{1}$ 0].

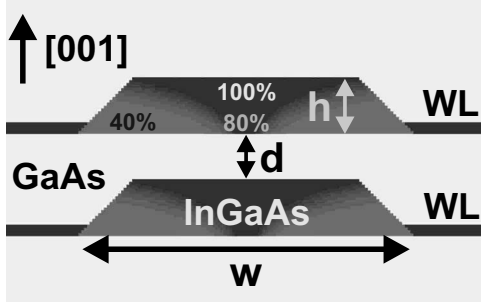


FIG. 1. Schematic cross section of vertically stacked (001)-grown InAs/GaAs double dot structure studied in this paper. We assume a height of $h=2.5$ nm, a width of $w=15$ nm, dot distances of $d=1.5$ or 2 nm, a wetting-layer (WL) thickness of 0.5 nm, and a realistic trumpet-shaped alloy profile within the dots (Ref. 31).

III. RESULTS: RESONANT TUNING OF EXCITON g FACTORS

We first discuss the molecular eigenstates for zero magnetic field as a function of the vertically applied electric field in terms of the individual electron and hole ground states. For dot distances $d \leq 2$ nm, the lowest molecular electron state ranges over both dots and forms an extended bonding state for all electric fields considered here. This is a consequence of the small electron mass and has been visualized in Fig. 2. By contrast, the individual dot hole states are more localized and therefore respond more sensitively to the electric field. The field tunes the energies of these individual dot hole states relative to each other. For negative electric field ($\mathbf{F} \parallel [00\bar{1}]$), the molecular hole ground state is predominantly localized in the lower dot (cf. Fig. 2) and vice versa for positive electric fields. For a particular field \mathbf{F}_{res} , the two ground states are tuned into resonance and form molecular bonding and antibonding orbitals with energies $E_{h,B}$ and $E_{h,A}$, respectively. This field strength \mathbf{F}_{res} is slightly nonzero because the strain field produces a small asymmetry between the individual dot energies.³⁰ For a dot separation of $d=1.5$ nm, our calculations give $\mathbf{F}_{\text{res}}=7$ kV/cm. For this dot

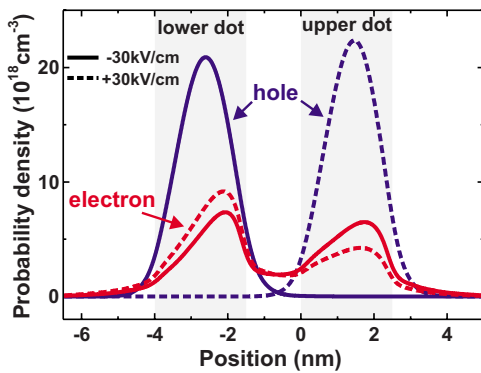


FIG. 2. (Color online) Cross sections of calculated molecular electron and hole ground-state probability densities for a dot separation of $d=1.5$ nm. The cross sections are taken at the dot center and run along the vertical [001] growth direction. In addition, we have applied a vertical electric field of +30 (solid lines) or -30 kV/cm (dashed lines) relative to the resonance field \mathbf{F}_{res} .

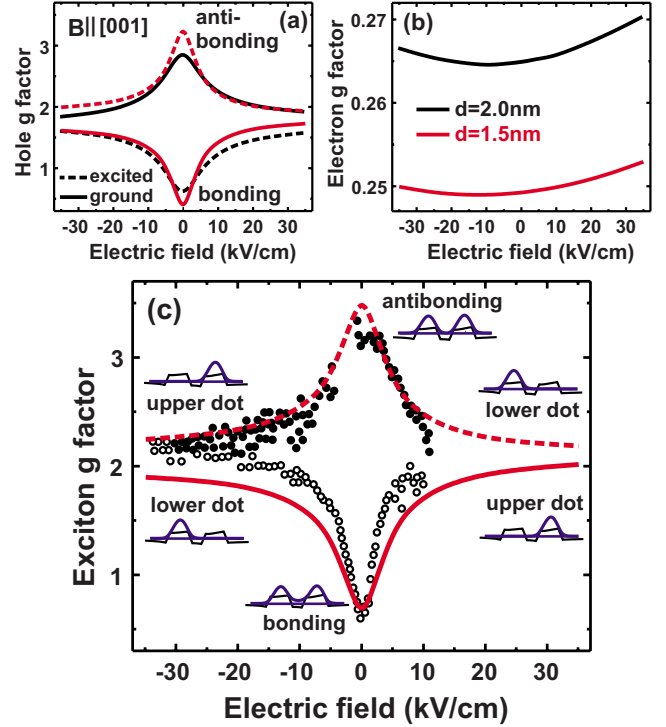


FIG. 3. (Color online) g factors of coupled quantum dots, for magnetic and electric fields lying in the vertical [001] direction. All electric field values in units of kV/cm are specified relative to the resonance field \mathbf{F}_{res} , as discussed in the main text. (a) Calculated hole g factors for ground state (full lines) and excited state (dashed lines). The black lines show results for dot separations of $d=2$ nm, while the red (gray) lines are for $d=1.5$ nm, respectively. (b) Calculated electron g factors for the ground state. Dot separations are taken as in (a). (c) Comparison of calculated neutral exciton g factors with experimental results from Ref. 18 (circles). The excitons are formed by an electron in the ground state and a hole either in the ground (full line) or first-excited state (dashed line). The dot separation is $d=1.5$ nm. The insets indicate schematically the probability density of the hole states for different electric field values.

separation, we find $(E_{h,B}-E_{h,A})/2=+0.6$ meV, which implies the bonding state to be the molecular hole ground state. By increasing the separation d between the dots to a value $d=2$ nm, we find the role of bonding and antibonding states to become reversed and we obtain $(E_{h,B}-E_{h,A})/2=-1.1$ meV. This is in good agreement with a previous theoretical result.³⁴ Experimentally, one finds a qualitatively similar trend but the crossover dot distance seems to lie at slightly larger values of the dot separation d .^{18,34}

We now turn to the molecular electron and hole g factors in the presence of a small vertical magnetic field $\mathbf{B} \parallel [001]$. In Fig. 3(a), we show the molecular hole g factors associated with the ground and first-excited state, respectively. The hole g factors can be tuned by more than 100% by the electric field and show a pronounced resonance behavior associated with the formation of bonding and antibonding hole states. Qualitatively, this resonance formation has been explained previously in terms of a simple model.¹⁸ Since, however, this work assumed incorrect signs of the bulk and single dot hole g factors, we present a brief discussion of our results. The

heavy-hole g factor in bulk GaAs is negative and given by $g_{hh}(\text{GaAs}) = -6\kappa = -7.2$ in terms of the Luttinger parameter κ .^{12,13,25} The present quantitative calculations show that the hole g factors associated with the isolated quantum dots are positive and approximately equal to +1.8. This result can be deduced from Fig. 3(a) in the limit of large positive or negative field where the molecular states are localized within the individual dots and the molecular coupling plays no role. We would like to point out that the present theory does predict negative hole g factors for larger quantum dots where quantum confinement is less pronounced.¹³ This is also in agreement with experiment.²⁸ For the present coupled quantum dots, the formation of bonding (antibonding) states as a function of the electric field increases (decreases) the overlap of the molecular states with the GaAs barrier region in between the coupled quantum dots which leads to a decrease (increase) in the molecular hole g factor. This effect is more pronounced for smaller interdot distances and this is shown in Fig. 3(a) for the two cases of $d=1.5$ and $d=2$ nm. We note that the figure exhibits a slight asymmetry between positive and negative electric fields which is related to the different strain fields felt by the two dots.³⁰ The g factor associated with the electron ground state remains almost constant for the entire range of fields as shown in Fig. 3(b).

Based on these calculations of electron and hole g factors, we can now predict the excitonic molecular g factor. In Fig. 3(c), we show the resulting effective exciton g factors [Eqs. (6) and (7)], formed by the electron ground state and the hole ground and first-excited state as a function of the electric field. The trends in the exciton g factors entirely reflect the trends of the hole g factors, whereas the electron g factor only shifts the absolute values slightly. To illustrate the resonant behavior of the exciton g factor, the insets in Fig. 3(c) mark the localization of the hole states in the coupled dots for the different electric field regimes. As can also be seen from the figure, our calculations are in excellent agreement with the experimental results from Ref. 18.

IV. RESULTS: GIANT g FACTOR SWITCHING

We now show that the hole g factors in coupled quantum dots can be electrically tuned by as much as 800% and effectively switched between almost zero and a finite value by applying a constant magnetic field in the growth plane rather than along the growth axis. Importantly, we find an unusually pronounced magnetic field anisotropy of the Zeeman splitting within the growth plane. As will be shown below, this is caused by the piezoelectric polarization associated with quantum dot molecules. In Fig. 4, the calculated molecular hole g factors for magnetic fields oriented along the planar directions $[110]$ and $[1\bar{1}0]$ are shown. Since the electron g factors remain constant ($g_e=0.45$) over the shown electric field range, the figure applies to exciton g factors as well. Analogous to the situation for vertically applied magnetic fields, we obtain a resonant reduction and enhancement of the g factors for the bonding and antibonding states, respectively. The molecular ground state [shown in Fig. 4(a)] is still localized in the upper and lower dot for large positive and negative electric field, respectively. In fact, we find the char-

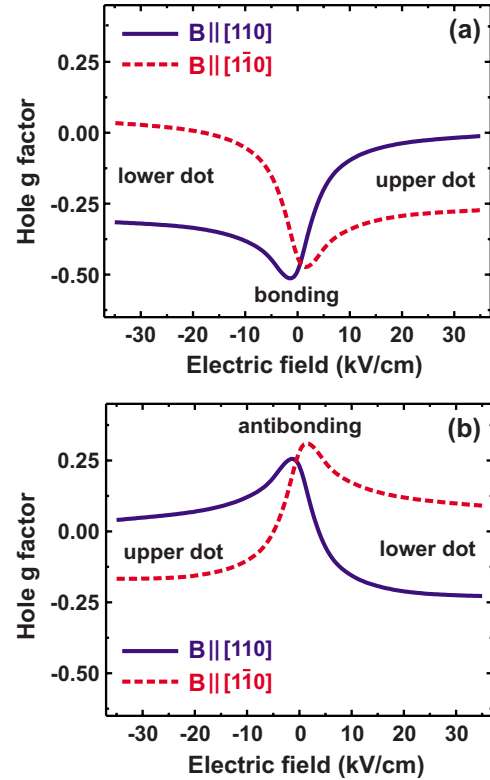


FIG. 4. (Color online) (a) Calculated molecular g factors of hole ground state as a function of vertically applied electric field (relative to the resonance field F_{res}) in kV/cm. The constant lateral magnetic field lies along the $[110]$ (full line) and $[1\bar{1}0]$ direction (dashed line), respectively. (b) Same for first-excited hole state. For large magnitudes of the electric fields, the molecular hole states are localized predominantly in either the lower or the upper dot, as indicated in the figure.

acter of this state to be almost independent of the modulus and direction of the magnetic field up to 10 T. For the first-excited state, the role of the upper and lower dots is reversed.

The results indicate a highly efficient bias induced switching of the molecular g factor between a value close to zero and a finite negative value for the extremal electric field values. This switching behavior is a robust effect and neither sensitive to small changes in the bias, as can be deduced from Fig. 4, nor to small changes in the quantum dot widths. Importantly, the calculations predict a pronounced anisotropy of the ground and excited-state hole g factors. By orienting the magnetic field along the $[1\bar{1}0]$ instead of the $[110]$ direction, the results indicate that the role of the upper and lower dot in the molecular states are effectively swapped. In summary, we find the following relations to hold for the hole ground state,

$$|g_{E \rightarrow +\infty}^{[110]}| \approx |g_{E \rightarrow -\infty}^{[1\bar{1}0]}| \ll |g_{E \rightarrow +\infty}^{[1\bar{1}0]}| \approx |g_{E \rightarrow -\infty}^{[110]}|. \quad (8)$$

Analogous relations can be given for the first-excited hole state. Since the g factors associated with the magnetic field directions $[110]$ and $[1\bar{1}0]$ cross each other at the electric field F_{res} , the Zeeman splitting becomes isotropic within the growth plane for this particular field value. To the best of our

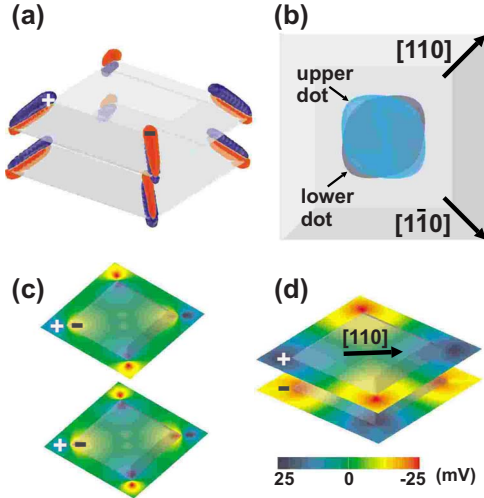


FIG. 5. (Color online) (a) Isosurface of calculated piezoelectric polarization charge densities of magnitude $\pm 1.5 \times 10^{19} \text{ cm}^{-3}$ near the overgrown quantum dots. Positive and negative charges are indicated in blue (dark gray) and red (light gray), respectively. (b) Isosurface of probability density of molecular hole ground state for an applied bias of +30 and -30 kV/cm, indicated in light blue (light gray) and dark blue (dark gray), respectively. The isosurface is chosen at 25% of the maximum density. The dot separation amounts to $d=1.5 \text{ nm}$. For these large positive and negative electric fields, the hole ground state is localized in the upper or the lower dot, respectively. (c) Cross sections of the calculated electrostatic potential that results from the piezoelectric charges for a dot separation of $d=24 \text{ nm}$. The cross sections are taken at half of the dot height. (d) Same as (c) for $d=1.5 \text{ nm}$.

knowledge, such a tunable and pronounced anisotropy of quantum dot related g factors has not been observed or discussed so far. In-plane anisotropies of electron g factors in single-quantum dots have been found to be quite small as expected.¹⁵ The present effect is caused by the piezoelectric charge distribution near the edges of the quantum dots that deform the hole charge distribution differently in the two coupled quantum dots that form the molecule. In the following, we will explain this effect in some detail.

For a truncated pyramid shaped buried quantum dot, there are piezoelectric charge dipoles located at the pyramidal edges.²³ The presently calculated piezoelectric charge distributions are shown in Fig. 5(a). These dipole charges lead to a potential profile that elongates the hole wave functions along one diagonal and compresses them along the perpendicular direction. For two vertically well separated quantum dots, this potential profile is very similar for both dots. In Fig. 5(c), we plot an overlay of two two-dimensional (2D) cross sections of the electrostatic potential onto the geometric dot profiles. The cross sections are taken at half of the quantum dot height in each dot. The dot separation is $d=24 \text{ nm}$ in this case. For a smaller dot separation, the multipole potential changes its character completely as shown in Fig. 5(d) for $d=1.5 \text{ nm}$. The individual quantum dot potential profiles are now rotated with respect to each other by 90° . In addition, the dot molecule behaves as a single vertical dipole at each corner of the pyramid rather than as two consecutive dipoles as in Fig. 5(c). In Fig. 5(b), we show a top

view of the two hole wave functions that lie in different quantum dots. They show a deformation that corresponds to the dipolar potential. The upper and lower hole wave function is elongated along the $[1\bar{1}0]$ and $[110]$ direction, respectively. The in-plane g factors in Fig. 4 follow this trend since they correlate with the spatial extent of the wave functions. This explains the anisotropy and the switching behavior of the ground and excited-state hole g factor.

V. EFFICIENT UNIVERSAL SPIN QUBIT GATE

In this section, we discuss an application of the strong magnetic field anisotropy together with the strong electric field dependence of the g tensor in quantum dot molecules. These two combined effects allow one to fully control the spin precession axis and therefore the spin polarization of a single hole in a quantum dot molecule. There are two prerequisites to achieve such a universal spin qubit gate. The first one is a static magnetic field along a direction of the dot molecule that is *not* equal to a principal axis of the hole g tensor. The other condition is a selective electric top gate that acts on the quantum dot molecule and applies a bias across the two coupled quantum dots. For individual quantum dots and electrons, such a full Bloch sphere control of the spin polarization has been predicted previously.¹⁶ However, we find the modulation of hole g factors in quantum dot molecules to be an order of magnitude larger than in individual quantum dots. Experimentally, this effect has only been observed in heterostructures for an ensemble of carriers so far.⁸ In addition, we find the g factors to form plateaus in their electric field dependence, making the spin manipulation less sensitive to slight variations in the applied voltage pulses.

We can write the Hamiltonian (4) in the form

$$H_h = \boldsymbol{\sigma} \cdot \boldsymbol{\Omega}_h, \quad (9)$$

where $\boldsymbol{\Omega}_h = 1/2\mu_B\hat{g}_h \cdot \mathbf{B}$ denotes the spin precession vector and the g tensor of the quantum dot molecule can be given explicitly in the Cartesian basis as

$$\hat{g}_h = \begin{pmatrix} \frac{g_h^{[110]} + g_h^{[1\bar{1}0]}}{2} & \frac{g_h^{[110]} - g_h^{[1\bar{1}0]}}{2} & 0 \\ \frac{g_h^{[110]} - g_h^{[1\bar{1}0]}}{2} & \frac{g_h^{[110]} + g_h^{[1\bar{1}0]}}{2} & 0 \\ 0 & 0 & g_h^{[001]} \end{pmatrix}, \quad (10)$$

where $g_h^{[110]}$, etc. are the elements of the g tensor along the principal axes. If a magnetic field is applied along the $[100]$ direction, a single spin in this field will start to precess around the axis \mathbf{e}_Ω , which is given by

$$\mathbf{e}_\Omega = \frac{\boldsymbol{\Omega}_h}{|\boldsymbol{\Omega}_h|} = \frac{1}{g_h^*} \left(\frac{g_h^{[110]} + g_h^{[1\bar{1}0]}}{2}, \frac{g_h^{[110]} - g_h^{[1\bar{1}0]}}{2}, 0 \right). \quad (11)$$

The unit vector \mathbf{e}_Ω is normalized by the effective hole g factor $g_h^* = |\hat{g}_h \cdot \mathbf{B}|/B$. This spin precession axis can be controlled by an applied vertical electric field. In Fig. 6, we plot the directions \mathbf{e}_Ω together with g_h^* as a function of the electric field, for the molecular hole ground state and the first-excited

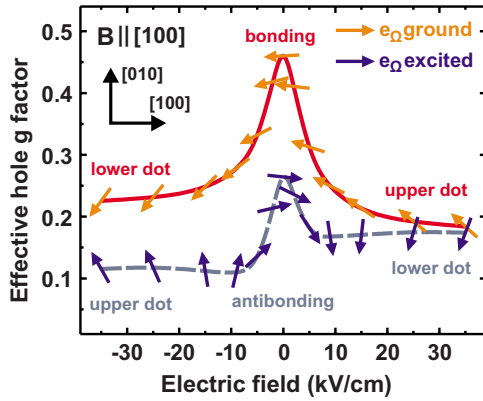


FIG. 6. (Color online) Calculated effective g factors and directions of spin precession axes (arrows) of hole ground state (solid line) and first-excited state (dashed line) as a function of the vertical electric field in kV/cm. The constant magnetic field lies in the horizontal $[100]$ direction.

state. For the molecular ground state, the electric field is able to rotate the precession axis \mathbf{e}_Ω by 90° from $[\bar{1}\bar{1}0]$ for large negative field magnitudes to the $[\bar{1}10]$ direction for large positive values. This pronounced tunability of \mathbf{e}_Ω can be deduced from Eq. (11) and Fig. 4 and is caused by the fact that one of the g factors associated with the magnetic field directions $[110]$ and $[1\bar{1}0]$ vanishes for large magnitudes of the electric field values. For the first-excited state, the axis can be rotated even by 270° . In both cases, the modulus of the g factor lies between those of the principal axes in Fig. 4 for all electric field values.

In order to fully control the spin of a carrier that is confined to a quantum dot molecule, two orthogonal precession axes are needed. These axes generate the two rotation angles that define any point on the Bloch sphere. For the present structure, one could use, e.g., the axes in Fig. 6 that can be associated with large positive and large negative electric field values, respectively. This concept allows universal quantum gating with a single electric gate on top of the structure and a static magnetic field.

VI. RESULTS: RESONANT ELECTRON g FACTORS

We have repeated the calculations in Sec. III for electrons but assumed a much larger interdot distance $d=10$ nm in

order to be able to localize a single electron in each dot separately for large positive and negative electric fields. For the magnetic field lying in the $[001]$ direction, we also obtain a resonant reduction and enhancement of the electron g factors for the bonding (B) and antibonding (A) states, respectively. However, the effect is much smaller than for holes and amounts to $g_e^A - g_e^B = 0.05$ only. For the in-plane directions $[110]$ and $[1\bar{1}0]$, the resonance effect is totally negligible. Even the addition of aluminum to the barrier material (which has been proposed in Ref. 18) did not increase the effect, in spite of larger difference between the g factors [$g_e(\text{AlAs}) = 1.52$, while $g_e(\text{GaAs}) = -0.44$]. The addition of indium [$g_e(\text{InAs}) = -14.8$] to the barrier only slightly enhances the resonance ($g_e^A - g_e^B = 0.1$, for 20% In and $d=15$ nm), simply because the delocalization of the electron state (in comparison to the hole state) renders its wave function fairly insensitive to reasonable electric fields. Thus, we conclude that electrons are less suitable for this type of g factor engineering in materials with small effective mass.

VII. SUMMARY

In summary, we have theoretically investigated electron, hole, and exciton g tensors of vertically stacked quantum dot molecules in vertical and lateral magnetic fields as a function of an applied vertical electric field. We are able to quantitatively explain the experimentally observed¹⁸ resonant enhancements of the g tensor components for vertical magnetic fields without any fitting parameters. For magnetic fields lying in the base plane of the quantum dots, we predict a very pronounced anisotropy in the hole g factors for $[110]$ and $[1\bar{1}0]$ magnetic field directions. In addition, we predict a bias induced g factor switching between almost zero and a finite value for constant magnetic field. Both effects are caused by the piezoelectric charges at the edges of the quantum dots that deform the eigenstates. This tunable anisotropy allows a full control of the spin polarization of a single hole in a quantum dot molecule by a gate voltage and thus the construction of a universal spin qubit gate.

ACKNOWLEDGMENTS

The authors acknowledge support from the Deutsche Forschungsgemeinschaft (Grants No. SFB 631 and No. SPP 1285), the Austrian Science Fund FWF (SFB IRON), and the Nanosystems Initiative Munich (NIM).

¹D. Loss and D. P. DiVincenzo, Phys. Rev. A **57**, 120 (1998).

²J. R. Petta, A. C. Johnson, J. M. Taylor, E. A. Laird, A. Yacoby, M. D. Lukin, C. M. Marcus, M. P. Hanson, and A. C. Gossard, Science **309**, 2180 (2005).

³M. Kroutvar, Y. Ducommun, D. Heiss, M. Bichler, D. Schuh, G. Abstreiter, and J. J. Finley, Nature (London) **432**, 81 (2004).

⁴F. H. L. Koppens, C. Buizert, K. J. Tielrooij, I. T. Vink, K. C. Nowack, T. Meunier, L. P. Kouwenhoven, and L. M. K. Vandersypen, Nature (London) **442**, 766 (2006).

⁵B. E. Kane, Nature (London) **393**, 133 (1998).

⁶H. W. Jiang and E. Yablonoitch, Phys. Rev. B **64**, 041307(R) (2001).

⁷G. Salis, Y. Kato, K. Ensslin, D. C. Driscoll, A. C. Gossard, and D. D. Awschalom, Nature (London) **414**, 619 (2001).

⁸Y. Kato, R. C. Myers, D. C. Driscoll, A. C. Gossard, J. Levy, and D. D. Awschalom, Science **299**, 1201 (2003).

⁹M. T. Björk, A. Fuhrer, A. E. Hansen, M. W. Larsson, L. E. Fröberg, and L. Samuelson, Phys. Rev. B **72**, 201307(R) (2005).

- ¹⁰T. Nakaoka, T. Saito, J. Tatebayashi, and Y. Arakawa, Phys. Rev. B **70**, 235337 (2004).
- ¹¹C. E. Pryor and M. E. Flatté, Phys. Rev. Lett. **96**, 026804 (2006); Phys. Rev. Lett. **99**, 179901(E) (2007).
- ¹²W. Sheng and A. Babinski, Phys. Rev. B **75**, 033316 (2007).
- ¹³T. Andlauer, R. Morschl, and P. Vogl, Phys. Rev. B **78**, 075317 (2008).
- ¹⁴M. Bayer, O. Stern, A. Kuther, and A. Forchel, Phys. Rev. B **61**, 7273 (2000).
- ¹⁵T. P. Mayer Alegre, F. G. G. Hernández, A. L. C. Pereira, and G. Medeiros-Ribeiro, Phys. Rev. Lett. **97**, 236402 (2006).
- ¹⁶J. Pingnot, C. E. Pryor, and M. E. Flatté, Appl. Phys. Lett. **92**, 222502 (2008).
- ¹⁷J. H. H. Rietjens, G. W. W. Quax, C. A. C. Bosco, R. Nötzel, A. Yu. Silov, and B. Koopmans, J. Appl. Phys. **103**, 07B116 (2008).
- ¹⁸M. F. Doty, M. Scheibner, I. V. Ponomarev, E. A. Stinaff, A. S. Bracker, V. L. Korenev, T. L. Reinecke, and D. Gammon, Phys. Rev. Lett. **97**, 197202 (2006).
- ¹⁹S. Birner, T. Zibold, T. Andlauer, T. Kubis, M. Sabathil, A. Trelakakis, and P. Vogl, IEEE Trans. Electron Devices **54**, 2137 (2007).
- ²⁰See <http://www.wsi.tum.de/nextnano> for obtaining the nextnano executables and related publications.
- ²¹L. D. Landau and E. M. Lifshitz, *Theory of Elasticity* (Pergamon, Oxford, 1959).
- ²²I. Vurgaftman, J. R. Meyer, and L. R. Ram-Mohan, J. Appl. Phys. **89**, 5815 (2001).
- ²³M. Grundmann, O. Stier, and D. Bimberg, Phys. Rev. B **52**, 11969 (1995).
- ²⁴A. Schliwa, M. Winkelkemper, and D. Bimberg, Phys. Rev. B **76**, 205324 (2007).
- ²⁵*Semiconductors: Intrinsic Properties of Group IV Elements and III-V, II-VI and I-VII Compounds*, Landolt-Börnstein, New Series, Group III, Vol. 22, Pt. A, edited by O. Madelung (Springer, Berlin, 1987).
- ²⁶O. Voskoboynikov, C. P. Lee, and O. Tretyak, Phys. Rev. B **63**, 165306 (2001).
- ²⁷C. F. Destefani, S. E. Ulloa, and G. E. Marques, Phys. Rev. B **70**, 205315 (2004).
- ²⁸M. Bayer, A. Kuther, A. Forchel, A. Gorbunov, V. B. Timofeev, F. Schäfer, J. P. Reithmaier, T. L. Reinecke, and S. N. Walck, Phys. Rev. Lett. **82**, 1748 (1999).
- ²⁹A. S. Bracker, M. Scheibner, M. F. Doty, E. A. Stinaff, I. V. Ponomarev, J. C. Kim, L. J. Whitman, T. L. Reinecke, and D. Gammon, Appl. Phys. Lett. **89**, 233110 (2006).
- ³⁰H. J. Krenner, M. Sabathil, E. C. Clark, A. Kress, D. Schuh, M. Bichler, G. Abstreiter, and J. J. Finley, Phys. Rev. Lett. **94**, 057402 (2005).
- ³¹P. Offermans, P. M. Koenraad, J. H. Wolter, K. Pierz, M. Roy, and P. A. Maksym, Phys. Rev. B **72**, 165332 (2005).
- ³²M. A. Migliorato, A. G. Cullis, M. Fearn, and J. H. Jefferson, Phys. Rev. B **65**, 115316 (2002).
- ³³J. J. Finley, M. Sabathil, P. Vogl, G. Abstreiter, R. Oulton, A. I. Tartakovskii, D. J. Mowbray, M. S. Skolnick, S. L. Liew, A. G. Cullis, and M. Hopkinson, Phys. Rev. B **70**, 201308(R) (2004).
- ³⁴M. F. Doty, J. I. Climente, M. Korkusinski, M. Schreiber, A. S. Bracker, P. Hawrylak, and D. Gammon, arXiv:0804.3097 (unpublished).